Wavelet-based clod segmentation on digital elevation models of a soil surface with or without furrows

Edwige Vannier, Richard Dusséaux, Odile Taconet, Frédéric Darboux

WAVELET-BASED CLOD SEGMENTATION ON DIGITAL ELEVATION MODELS OF A SOIL SURFACE WITH OR WITHOUT FURROWS

E. Vannier[1*], R. Dusséaux[1], O. Taconet[1], F. Darboux[2]

[1] LATMOS/IPSL, Université de Versailles St Quentin,
11 boulevard d'Alembert 78280 Guyancourt, France

[2] Université de Lorraine, Inra, LSE, F-54000 Nancy, France

* Corresponding author: phone: + (33) 180285095, email: edwige.vannier@latmos.ipsl.fr

Declarations of interest: none.

Abstract

Soil surface roughness is a key factor for our understanding and modelling of geomorphologic processes related to exchanges of soil, water and gas. It has an impact on soil properties and tillage outcome. Soil surface roughness can be characterized both globally and locally. The interest of clod segmentation is to allow for both characterizations. Segmenting clods on a digital elevation model (DEM) of a soil surface is a complex problem because soil surfaces are complex surfaces of several level of roughness and because considering elevations results in smooth and poorly contrasted images. However, a DEM in 3 dimensions gathers more information than a profile of 1 dimension or an image of 2 dimensions.

Multiresolution analysis has shown interest for roughness analysis of complex surfaces. We have used it to introduce a new approach for soil roughness analysis and to lay the foundations for clod segmentation. In this paper, we propose a complete wavelet-based approach for accurate clod contour delineation. It relies on several steps: detecting clods on the surface approximations by a supervised detection of local maxima, validating and merging the detections by shape and overlap tests, delineating the clod contours by intersecting locally the soil surface elevations with the estimated plane of the clod base and validating the contours by detecting and correcting the wrong patterns, with statistical pattern recognition. This segmentation method was evaluated in several roughness conditions, made in the laboratory, by comparison with other segmentation method. An indicator of goodness of agreement was introduced for this purpose.

This wavelet-based segmentation method showed robustness to the presence of furrows and to the smoothing by rainfall and showed ability to retrieve clod diameters.

Key words: random roughness, 3D digital elevation model, multiresolution analysis, statistical pattern recognition, clod size

1 Introduction

The soil, being at the interface of the hydrosphere and the atmosphere, plays an important role in exchanges of soil, water and gas and geomorphologic processes. The role of soil surface roughness in the geomorphologic processes at small scale is commonly acknowledged, (for example Garbout et al., 2013, Bretar et al., 2013, Thomsen et al., 2015, Martinez-Agirre et al., 2016, Gilliot et al., 2017, Vannier et al., 2018 a, Zhao et al., 2018, Schapel et al., 2019). In agricultural fields, the soil surface roughness is shaped by tillage operations and is a result of soil and water mechanisms interaction and feedback. It is related to soil moisture and fertility (Gilliot et al., 2017, Zhao et al., 2018, Schapel et al.,

2019). It is usually characterized by several indices, estimated on profiles or images of the soil, characterizing the surface as a whole (Kamphorst et al., 2000, Taconet and Ciarletti, 2007, De Oro and Buschiazzo, 2011, Dusséaux et al., 2012, Smith, 2014). Roughness parameterization is still in question (Martinez-Agirre et al. 2016 and Gilliot et al. 2017). A second approach of the surface roughness considers the local irregularities such as aggregates, clods and depressions (Sandri et al., 1998, Darboux et al., 2001, Kamphorst et al., 2005, Arvidson and Bölenius, 2006, Bogrekci and Godwin, 2007, Vannier et al., 2009, Wang et al., 2011, Garbout et al., 2013, Taconet et al., 2013, Chimi-Chiadjeu et al., 2014, Jensen et al., 2016, Ajdadi et al., 2016, Vannier et al., 2018 a and b, Schapel et al., 2019).

The development of stereovision from photogrammetry or laser scanning allows for more and more studies based on digital elevation models (DEMs). Analysing elevation changes from DEMs can be interesting at different scales and in various contexts (Takken et al., 2001, Darboux et al., 2001, Jester and Klick, 2005, Blaes and Defourny, 2008, Haubrock et al., 2009, Ahmad Fadzil et al., 2012, Bretar et al., 2013, Jensen et al., 2016, Gilliot et al., 2017). However, as some baseline roughness indices were defined from 1D profiles, the potential of the three dimensions is not always exploited. In our recent studies, we showed that millimetric DEMs allow for both local and global characterization of soil surface roughness (Dusséaux et al., 2012, Taconet et al., 2013, Chimi-Chiadjeu et al., 2014, Vannier et al., 2014, Vannier et al., 2018 a and b).

The soil cloddiness can be quantified with the size distribution of the aggregates and clods. It serves to characterize soil quality produced by tillage and to control microrelief changes due to rainfall impact (Sandri et al., 1998, Arvidson and Bölenius, 2006, Bogrekci and Godwin, 2007, Wang et al., 2011, Garbout et al., 2013, Jensen et al., 2016, Ajdadi et al., 2016, Vannier et al., 2018 a and b) or control concentration of organic carbon (Schapel et al., 2019). Segmenting the clods is a complex problem because they can be dimly demarcated or embedded with each other or in another piece of relief. In (Vannier et al., 2009) we showed that it is difficult to automatically detect clods of a large size range in natural soil

surfaces recorded in the field. In the present study, we address the problem of segmenting clods in DEMs of laboratory made soil surfaces, with or without furrows, with different clod sizes and spacing, at initial stage and after roughness evolution caused by rainfall events. Let us underline that contrary to the 2D images usually processed for edge detection or segmentation, a 3D DEM of a soil surface has a lower contrast. In the gradient-based method of segmentation introduced in (Taconet et al., 2010), at least 90% of the gradient values should be retained in order to detect the clods. In (Chimi-Chiadjeu et al., 2014), a transformation of the image of the surface should be effected before the rough estimation of the clod contours by watershed segmentation. In this paper, we have chosen a geometrical approach, in order to take advantage of the three dimensions of the DEMs. Multiresolution analysis has shown interest for roughness analysis of complex surfaces (Josso et al., 2001 and 2002, Vannier et al., 2006, Fernandez-Diaz et al. 2010, Ahmad Fadzil et al., 2012, Labarre et al., 2017). This approach enabled us to detect the clods on soil surface DEMs with satisfactory sensitivity (84%) and specificity (94%) and to localize clods by their summit and extensions in two directions (Vannier et al., 2009). In this paper, we propose a complete wavelet-based approach, relying also on statistical pattern recognition, in order to reach an accurate delineation of the clod contours. The section materials and methods introduces the data base used in this study, the segmentation method and its evaluation. Then segmentation results are presented and compared with other segmentation methods in the result and discussion section.

2 Materials and methods

2.1 Soil preparation and measurement

The database used in the present study is composed of laboratory made soil surfaces prepared with two different soils and a various range of sieved clods, in order to evaluate the segmentation method in various roughness conditions.

98 In order to do so, two trays of 50 x 50 cm^2 were prepared with loose silt loam soil for 10 cm
99 depth. One of them had a nearly planar surface (P) and the other one was shaped with
100 gentle furrows every 8 cm (F). Then air-dried clods collected in the field were set upon the
101 two soil surfaces, with various sizes and spacing to reproduce different roughness conditions
102 (Figure 1). These trays were subjected to controlled rainfalls with a laboratory rainfall
103 simulator similar in design to the one presented in (Foster et al., 1979) also described in
104 (Vannier et al., 2018 a and b). This simulator was equipped with oscillating nozzles
105 producing raindrops of 1.5 mm mean diameter at an adjustable number of sweeps per
106 minute to set the desired intensity. For each tray, we retained 3 stages of roughness: the
107 initial stage, the stage after 2 hours of rainfalls at 33 $mm.h^{-1}$ intensity, and the stage after 3
108 additional hours at 42 $mm.h^{-1}$ intensity. The DEM of each stage of surface roughness was
109 recorded with the laser scanner described in (Darboux & Huang, 2003, Vannier et al. 2018 a
110 and b). Summarily, the principle of recording relies on a laser producing a line on the soil
111 surface and a CCD camera set at an angle to measure the surface geometry along a profile
112 in the y-z planes. By moving the device along the x-axis, the whole surface elevations are
113 obtained. The accuracies were 0.5 mm in x and y axes, and 1 mm in z axis. In order to
114 introduce geometrical criteria for statistical pattern recognition used along with multiresolution
115 analysis in clod segmentation procedure (see section 2.2.2), the data were resampled at 1
116 mm resolution in x y z. We also referenced the elevations to be positive. Hereafter, the 6
117 DEMs are denoted P0, P1, P2 and F0, F1, F2 for the initial stage, the stage after one rainfall
118 event and the stage after two rainfall events for the planar soil surface and the furrowed soil
119 surface respectively (Fig. 2).

120 Then we added a third tray of 50 x 50 cm^2 prepared with Lavaur clay loam soil for 10 cm
121 depth, shaped with an oriented roughness of centimetric ridges and furrows. Air-dried 2-cm-
122 sieved aggregates were thrown upon and formed a thick cloddy structure. Figure 3 shows a
123 photo and the DEM of this one sieve range soil surface, called SR.

2.2 Wavelet-based clod segmentation

2.2.1 Multiresolution analysis of the soil surfaces

The detection and approximate localization of clods was performed according to the wavelet-based detection method introduced in (Vannier et al. 2009). This method first processes to a multiresolution decomposition of the soil surface by wavelet transform.

Let us now recall the basis of the multiresolution analysis theory, (Mallat, 1989, Daubechies, 1992, Choksi, 2018), and introduce the notations. It is possible to decompose the surface elevations $z=S(x,y)$, into one approximation $A_N(x, y)$ and the sum of N details $D_1(x, y)$, …, $D_N(x, y)$, at different levels N:

$$S(x, y) = A_N(x, y) + \sum_{n=1}^{N} D_n(x, y) \quad (1)$$

The approximations and details of the surface are computed by recurrence:

$$S(x, y) = A_0(x, y) \quad (2)$$

$$A_{n-1}(x, y) = A_n(x, y) + D_n(x, y) \quad (3)$$

Where $D_n(x, y)$ denotes the summation of the horizontal, vertical and diagonal detail surfaces:

$$D_n(x, y) = D_{Hn}(x, y) + D_{Vn}(x, y) + D_{Dn}(x, y) \quad (4)$$

At each intermediate level n, $A_n(x, y)$ and $D_n(x, y)$ were computed with the decimated and undecimated algorithms, which produce sub-images having the same size as the original image. Indeed, the frequency plan is subdivided into two parts of low and high frequencies along each dimension x and y. The approximation is the low-low frequency part, the horizontal detail the high-low frequency part, the vertical detail is the low-high frequency part, and the diagonal detail is the high-high frequency part. We used the orthogonal wavelet family selected in (Vannier et al., 2009), with mother wavelet Daubechies of level 9 (Daubechies, 1992).

147 Then, a supervised local maxima extraction was performed on the retained surface
148 approximations and the results of all extractions were merged. As a result, the individual
149 clods of the soil surface were localized by their summit and extensions in the x y plane. The
150 whole procedure is detailed in (Vannier et al. 2009).

151 It was shown that the successive approximations of the soil surface contained most of the
152 surface energy. Selecting the proper levels of approximations, depending on the roughness
153 scale of the soil surface, allowed for the detection and localization of the range of clods
154 present on the soil surface. As an example, for the seedbed considered in (Vannier et al.
155 2009), containing clods of diameters less than 53 mm, the levels of approximations A3 and
156 A2 were relevant. Due to clod proximity, level A4 was not suitable. With the present silt loam
157 surfaces, containing spaced clods of diameters up to 76 mm, it was necessary to include the
158 levels A4 and A5, in order to detect also the larger clods. And with the Lavaur clay surface,
159 containing very small and nearby clods, the levels A1 to A3 were selected.

160 ### *2.2.2 Statistical pattern recognition of clods*

161 The accurate delineation of the clod contours was done by intersecting locally the soil
162 surface with the estimated plane of the clod base. This process relies on several steps of
163 validation, based on statistical pattern recognition of a good clod segmentation and improper
164 object segmentation. The algorithm is shown in Fig. 4. An introduction to statistical pattern
165 recognition can be found in (Webb, 2002). In the present study, linear discriminant analysis
166 was sufficient to detect the wrong patterns.

167 The first test of goodness of intersection of the local surface with its mean plane (Fig. 4, line
168 5) detected the cases where the contour does not suit the clod due to erroneous inclination
169 or level of the plane. It resulted in partially squared contour as illustrated in Fig. 5a. This
170 pattern could be detected using the quantiles of coordinates x_c and y_c of the data points of
171 clod contour at minimum, 12.5%, 87.5% and maximum. We had a wrong pattern if two
172 quantiles were equal for x_c or y_c. Then, the inclination and height of the mean plane were
173 refined when needed.

The second test of goodness of intersection (Fig. 4, line 6) checked for requirement of the local surface to be extended in one or more than one direction. As illustrated in Fig. 5b, a too small local surface due to inadequate extensions of detected clod, caused straight borders in the clod contour. These lines were detected by thresholding the percentage of abscissa (or ordinates) equal to their minimum or maximum value. The local surface was then extended a little in the direction given by straight borders and the test repeated until no extension was required.

The third test (Fig. 4, line 7) aimed at detecting blocks of clods (as in Fig. 5c) when the clods were very close together. It could occur also due to furrow interference or presence of small aggregates near a larger clod. At initial stage, we would like to distinguish the individual clods. A block of clods was characterized by an elevated circularity and a gradient of clod elevations with more than one mode or one enhanced mode. In that case, the clod contour was searched as an iso-gradient or an iso-elevation contour.

The last test (Fig. 4, line 10) detected the squared like contours (as in Fig. 5d), where the clod was partly squared. Again, the percentages of abscissa or ordinates equal to their extremum value were computed. They were compensated for the clod perimeter and diameter and thresholded. In that case, the level of the mean plane was elevated and the clod contour re-evaluated. If a wrong pattern was obtained again, the contour was discarded as it is the case in the example in Fig. 5d).

2.3 Evaluation of segmentation method

For the silt loam soil surfaces P0, P1, P2, F0, F1 and F2, we had a reference of contours drawn by hand on a photo of the surface, with visual check looking at the surface in the laboratory. This reference was scanned. In order to make a clod by clod survey, the studied area was reduced to 30 x 30 cm^2 and the DEMs were shown in mm. The total number of clods was near 300 for these silt loam soil surfaces.

We evaluated the wavelet-based segmentation by comparison with the hand-made segmentation and two other segmentation methods, the contour-based approach introduced in (Taconet et al. 2010) and the threshold method used in (Vannier et al. 2018 a and b). The hand-made segmentation is subjective and has a bias due to contours delineation on 2D photos of the soil surfaces. The threshold method detects objects having elevations above a fixed threshold. It therefore requires that the clod support is flat and horizontal, which is not the case of a furrowed surface. However, it is a solid objective reference for a planar horizontal surface. The contour-based method researches iso-elevation contours passing through high gradient data points. It has the advantage to be very close to the threshold method on a planar surface and to be still applicable on a clod support of variable heights. It nonetheless reaches its limits if the clod support is too much tilted [Chimi et al., 2013].

The reference index of segmented region similarity is Jaccard index also called Intersection over Union (IoU) (Shen and Zeng, 2019 and Zhang et al., 2019). It can be interpreted as an overlap rate between the two segmented regions. These indices were computed with one set of segmented contours serving as reference. The IoU of regions delimited by contours k and l was denoted $\tau_{k,l}$ and defined as in (Chimi et al. 2013):

$$\tau_{k,l} = \frac{\mathcal{A}_k \cap \mathcal{A}_l}{\mathcal{A}_k \cup \mathcal{A}_l} \quad (5)$$

where $\mathcal{A}_k$ is the area delimited by the contour k of the clod in the first set of segmented contours and $\mathcal{A}_l$ is the area delimited by the corresponding contour l of the clod in the second set of segmented contours. The denominator $\mathcal{A}_k \cup \mathcal{A}_l$ makes the overlap rate stricter than taking just the area of the reference contour $\mathcal{A}_k$. However, it is necessary to prevent the case where $\mathcal{A}_l$ would be very large including $\mathcal{A}_k$, giving an overlap rate of 100% whereas the contours would be of very different sizes. That is why the regions are considered similar if the IoU is above 50% and dissimilar otherwise (Wand et al., 2019). The average IoUs are usually reported. However, the average is limited to characterize the

segmentation results on a wide number of objects, therefore it is usually associated with other indices of performance.

The IoU is sensitive to the discretization of the contours due to DEM accuracy and is stricter for small clods than for large ones. As an example, figure 6 shows two contours of radius respectively of 3 mm and 6 mm, and the same contours translated by 1 mm. The visual agreement is quite satisfactory and yet the IoUs are respectively of 58% and 76%.

For the planar surfaces P0, P1 and P2, we used the hand-made segmentation and the threshold segmentation as references. For the furrowed surfaces F0, F1 and F2, the references were the hand-made segmentation and the contour-based segmentation applied on a detrended surface, where the average of the rows has been removed. Let us specify that both the hand-made and the wavelet-based segmentations were performed on the original furrowed surfaces.

Then we also used other indices such as the clod coverage, which is the ratio between the total area delimited by clod contours and the product of DEM horizontal dimensions, and the mean weighted diameter (MWD) as defined in (Taconet et al. 2010):

$$MWD = \sum_{i=1}^{N} \mathcal{D}_i . s_i \quad (6)$$

Where N is the total number of clods, $\mathcal{D}_i$ is the equivalent diameter of clod i (estimated here from the area of clod, considered as a disk) and s_i is the fraction of the area covered by clod i:

$$s_i = \frac{\mathcal{A}_i}{\sum_{k=1}^{N} \mathcal{A}_k} \quad (7)$$

And, we introduce a fourth index based on the weighted cumulative distribution function (WCDF) of the IoUs of the common segmented clods:

$$F_w(\tau) = \sum_{if\ \tau_{k,i}<\tau} s_k \quad (8)$$

In (Chimi et al. 2013), we computed the cumulated distribution function (CDF) of the IoUs, called overlap rates, which shows the probability that $\tau_{k,l} < \tau$, for $\tau \in [0\ 1]$. In this paper, we

used rather weighted IoUs and we defined a quantitative index illustrating the low probability to have a small IoU and the high probability to have a high IoU.

The difference between two segmentation methods is quantified with the help of the area under curve (AUC) of $F_w(\tau)$. The smaller the AUC, the greater the agreement between the segmentation methods. The goodness of the agreement can thus be defined as:

$$G = 1 - \int_0^1 F_w(\tau) d\tau \quad (9)$$

The equality $G = 100\%$ would reflect the perfect accordance between all contours and $G = 0\%$ the total discrepancy. This index is very strict and reflects the overall distribution of the IoUs. It can be considered satisfactory if greater than 0.5.

For the Lavaur clay loam soil surface SR, the clods are numerous, very small and very close together, which hinders a clod by clod survey. A smaller area of 20 x 20 cm^2 was used to run the wavelet-based segmentation and retrieve the clod equivalent diameters and an even smaller part of the surface was segmented manually. We compared the MWD obtained by segmentation to the one measured with a sample of this soil in the laboratory. The number of clods was near 170 on the studied area.

3 Results and discussion

First of all, there is an overall good agreement between the segmentation methods for the silt loam soil surfaces. The mean IoUs range from 54.7%, for F2 to 85.5%, for P0 (see Table 1). As the hand-made segmentation had its own bias, the IoUs were also estimated with an automatic method serving as reference when possible. In average, for the wavelet-based method, with all possible references, the mean IoU amounts 71.1%, which is in the order of magnitude of encountered mean IoUs in the literature (Shen and Zeng, 2019 and Zhang et al., 2019). The variations of mean IoUs from one surface to another will be explained with the help of the other indices later on. Let us now look at segmentation results in more detail.

The segmentation results for the surface P0 can be seen in Figure 7. The three automatic segmentation methods are quite close to the hand-made segmentation. We notice that the contour-based approach (in blue) is very close to the threshold method (in green). Indeed, the contour-based method captures contours defined as level lines passing through high gradient points. If the clods are set upon a horizontal surface, the level lines are of very low elevation. There is an exception for clod 31 (x=175, y=225), which is a two-summit clod that have been captured by the contour-based approach instead of the clod base. Only the larger summit contour was kept for the evaluation. The wavelet-based method (in magenta) is closer to the hand-made segmentation than to the threshold one and tends to detect little more clods.

For the surfaces F0, F1 and F2, the presence of furrows does not allow for thresholding at constant elevation. The compared automatic method is the contour-based approach applied on a detrended DEM, where the ridges and furrows were estimated as an average of the DEM along the lines and removed. The effect of this detrending is strengthening the contour-based approach (Fig. 8, in blue). We can see a few contours (in black) on the ridges between the furrows that are not clod contours, for example numbers 7 (x=240, y=60) and 40 (x=160, y=160), which are rather grapes of large aggregates melted with the ridge, or 2 (x= 170, y= 225) that exceeds true clod border. However, the true clod 44 (x=45, y=150) in a furrow, was no more detected after detrending. Two clods (i.e. 19 (x=45, y=230) and 37 (x=50, y=290)) are difficult to segment by the contour-based approach, with or without detrending. We can discuss the meaning of the large aggregates more or less captured or not. For a visual survey, we can say that the minimum diameter of an aggregate should be at least 6 or 7 mm. Figure 9 shows the contours obtained with the wavelet-based method on the raw DEM (magenta) and with the contour-based approach on the detrended DEM (blue). The hand-made segmentation is in yellow dotted line. We can see that most of the contours of large clods are in good agreement. Some small clods or large aggregates were detected by one automatic method and not the other. The contour-based method captured some large

aggregates located in the furrows, on the border of the ridges or on the ridges. The wavelet-based method was able to capture the clod numbered 44 (x=45, y=150) in Figure 8, captured some other large aggregates on the ridges, but captured also two mentioned grapes of aggregates melt with the ridge (x=160, y=160, and x=90, y=260) numbered 40 and 47 on Figure 8.

The clod coverages, estimated with the different segmentation methods, are shown in Table 2, and the MWDs in Table 3. We can see the overall agreement of the methods. The effect of rainfall impact is first an increase of clod coverage and MWD (from P0 to P1 and F0 to F1) and then a decrease of clod coverage due to disappearance or erosion of the smaller clods, and a stabilization of MWD (from P1 to P2 and F1 to F2), which give more weight to the larger clods. We can notice than the wavelet-based method tends to underestimate the MWD due to difficulty to capture the borders of the very large clods (see Figure 6). The higher clod coverage for P0 is due to the detection of more small clods. The lower MWD of contour-based method for P0 can be explained by the mis-segmentation of a very large two-summit clod. For P2, MWD is overestimated by threshold method because it captured three blocks of nearby clods (8, 15, 18) while the other segmentation methods segmented them as single clods by (see Fig. 10). For the different stages of furrowed surface F0, F1 and F2, we have comparable MWDs for contour-based and wavelet-based segmentations but slightly higher clod coverage by wavelet-based method. This can be explained by the fact that contour-based method detects generally less clods than wavelet-based method. In particular, after two rainfall events, the number of segmented clods decreased a lot due to erosion, resulting in poorly shaped residual clods (see Fig. 11). Therefore, the MWD computed with contour-based method for F2 is likely overestimated, due to deficit of middle-size clods.

Table 4 gathers the estimated goodness of agreements (eq. 9) between the segmentation methods for the 6 roughness conditions. The three automatic segmentation overlap rates rank at good level of goodness when compared to hand-made segmentation. The higher score appears to be that of the threshold method, which is in agreement with the hand-made

method at 88.2% for planar surface at initial stage P0. When the threshold method is the reference for the three stages of the planar surface, we can see the robustness of the wavelet-based method, which has comparable or even better goodness of overlap rates. For both references, we notice a low decrease of goodness with the roughness smoothing and lowering due to rainfall. An explanation parameter is the size reduction of some clods. The mean IoU is more sensitive to clod size than G, however if the larger clods are not suitably segmented, the stabilizing property of G is lessened. It is the case, for P2, with the wavelet-based segmentation, leading to lower values of G. When considering the furrowed surfaces F0 to F2, G has less variations than mean IoU and the increase followed by a decrease of these parameters can be explained by the proportion of small clods in the surface.

When the contour-based method is the reference for the three stages of both planar and furrowed surfaces, a noticeable point is that the wavelet-based method performed well, segmenting clods on the raw DEMs while the contour-based method needed a detrending of the furrowed surfaces. Comparing the wavelet-based method to the contour-based method leaded to globally better goodness of agreement than comparing the wavelet-based method to the threshold method, because these two segmentation methods are sensitive to the slope of the clod shape from the summit to the border. For P0, the agreement score is lower, possibly due to the sensitivity of the segmentations to the small grains of the surface and to the difference of contours on a large two-summit clod. For P1 and F1 the smoothing action of rainfall enhanced the agreement score because the borders are less rough but still well defined and because some small clods have disappeared. At final stage, there were less common clods segmented because the residual clods are poorly shaped (see Fig. 11). The clods segmented by the wavelet-based method on F2 were present at an earlier stage, except one (x=95, y=80) forming a bump on a ridge. That means that the contours are meaningful. The interest of the wavelet-based method relies in its ability to keep on segmenting clods whatever the roughness conditions, with or without furrows, at initial stage or after rainfall events. This method performs better for clods than for large aggregates. In

354 average, for the wavelet-based method, with all possible references, the mean value of G is
355 77.5 % whereas the mean IoU amounts 71.1%. This higher score suits well to the visual
356 agreement seen in the figures 7, 9, 10 and 11, and to the small root mean squared error
357 (RMSE) of MWDs of 4 mm when comparing the wavelet-based to the hand-made derived
358 diameters (see table 3). Therefore, it is a more robust performance indicator when changing
359 the roughness condition by adding furrows or subjecting the surfaces to rainfall (see tables 1
360 and 4). It reflects more the segmentation performance than the DEM resolution and the clod
361 size effect as the mean IoU.

362 Let us now focus on the ability of wavelet-based segmentation to derive suitably the clod
363 diameters. We already mentioned the low RMSE of 4 mm in estimating MWDs of the 6 silt
364 loam DEMs. As a comparison, in Bogrekci and Godwin, 2007, the lowest RMSE between
365 sieve-derived and 2D image-derived MWDs was 14 mm. In our study, for the Lavaur clay
366 loam surface, the sieve range was 2 cm. Unfortunately, the sieved-derived MWD was not
367 measured for this soil. With hand-made segmentation, the minimum diameter is 7.0 mm, the
368 maximum diameter 24.3 mm, and the MWD 15.9 mm. With the wavelet-based segmentation,
369 some clods were missed or were segmented as a block of clods instead of single clods (see
370 Figure 12). The minimum diameter is 7.2 mm and the maximum diameter 23.3 mm, which is
371 very good agreement with the hand-made segmentation. The overall estimated MWD is 14.2
372 mm, which is in good agreement with hand-made estimation with a relative deviation of 10.7
373 %. We assume that hand-made segmentation is difficult with such small and nearby clods so
374 that it was performed on a small area where the clods were well defined and likely larger
375 than in other areas. So, the hand-made derived MWD was likely slightly over-estimated. The
376 wavelet-based derived MWD was nevertheless a little under-estimated as it was already the
377 case for the silt loam surfaces in table 3.

378 The silt loam surfaces present a wider range of clod diameters. In order to compare our
379 results with other methods available in the literature, we considered the total of 113 clods
380 from surfaces P0 and F0 at initial stage. Figure 13 shows the equivalent diameters derived

381 from wavelet-based and hand-made segmentations. We can see that they are close to the
382 diagonal. The linear fit gave $y = 0.86x + 3.8$, with R^2 = 96%. That is to say that the derived
383 diameters are highly correlated, with a slope quite close to 1 and an intercept quite close to
384 0. In Sandri et al. 1998, the linear regression of MWDs derived from 2D image segmentation
385 and from sieves gave $y = 1.02x + 3.9$, with R^2 = 81%. The slope is closer to one but R^2 is
386 lower than in present study. In Bogrekci and Godwin, 2007 , the linear regression of MWDs
387 derived from 2D image segmentation and from sieves gave $y = 1.21x$, with R^2 = 96%. Here,
388 the intercept is exactly 0 but the slope is higher than in present study. On the whole, our
389 results are comparable to that of the literature, and the main advantage, is having the
390 individual clod diameters instead of MWDs. Let us notice that in the cited papers of the
391 literature, the linear regressions were estimated along fractions of clod size, which introduced
392 an average effect enhancing the accuracy of the fit. So, we also gathered the clods in ten
393 groups of clod size, with medians of fractions: 9.0, 12.5, 13.9, 15.7, 18.2, 20.0, 22.8, 26.3,
394 28.8, and 36.1 mm. The linear regression on these fractions of clods leaded to $y = 0.93x +$
395 1.9, with R^2 = 99%, which is globally better than the cited results.

396 Segmenting soil clods on a DEM is a complex problem because 1) soil surfaces are complex
397 surfaces of several levels of roughness and 2) considering elevations results in less contrast
398 than pixel brightness in a 2D image. However, a 2D image can have some bias due to the
399 projection of a 3D volume onto a plane with a given lighting and does not allow to estimate
400 clod volume. That is why different approaches taking benefit of the three dimensions of a
401 DEM have to be developed. In the present paper, we adopted a geometrical point of view
402 relying on multiresolution analysis and statistical pattern recognition. The segmentation was
403 based on geometrical properties of the objects to be detected. The evaluation of its
404 performance is linked to DEM accuracy and to clod size. When the size of clods decreases,
405 the proposed approach reaches its limits. Indeed, the properties of clods and aggregates are
406 quite different and the approaches performing well for small aggregates as in (Ajdadi et al.,
407 2016), reach their limits when considering larger aggregates or clods and conversely.

4 Conclusion

In this paper, we developed a wavelet-based method to segment the contours of clods on DEMs of seedbed-like surfaces made in the laboratory with two different loams. The presence or absence of furrows, different sizes and spacing of clods and the use of a rainfall simulator allowed us to create different roughness conditions. We introduced a goodness of agreement index in order to compare the proposed method with other segmentation methods and computed also the mean IoU, clod coverage and mean weighted diameter. When the size of clods decreases, the proposed approach reaches its limits. Nevertheless, the wavelet-based method showed ability to keep on segmenting clods whatever the roughness conditions, with or without furrows, at initial stage or after rainfall events. It also showed ability to retrieve clod diameters with very good accuracy. It is therefore an efficient method that allows in particular to detect the contours of clods deposited on furrows.

Soil roughness is a key factor for understanding and modelling soil water-interactions and soil erosion. It can be estimated by several parameters, and characterized both locally and globally. Estimating the soil cloddiness is one way of evaluating the soil surface roughness. It is especially important for evaluating the soil quality after tillage operations, and for soil conservation decisions. A reliable automatic clod segmentation on a DEM opens perspectives for clod size distribution estimation and for numerical soil surface generation.

Funding: This study was funded by the French program: “Programme National de Télédétection Spatiale” (A02010-499016).

References

Ahmad Fadzil, M.H., Sathyamoorthy, D., Asirvadam, V.S., 2012. Computing surface roughness of individual cells of digital elevation models via multiscale analysis. Computers and Geosciences 43, 137-146.

Ajdadi F.R., Abbaspour-Gilandeh Y., Mollazade K., Hasanzadeh R.P.R., 2016. “Application of machine vision for classification of soil aggregate size”, Soil and Tillage Research 162, 8-17.

Arvidsson, J., Bölenius, E., 2006. Effects of soil water content during primary tillage – laser measurements of soil surface changes. Soil and Tillage Research 90, 222-229.

Blaes, X. and Defourny, P., 2008. Characterizing bidimensional roughness of agricultural soil surfaces for SAR modelling: *IEEE Transactions on geoscience and remote sensing*, vol. 46, pp. 4050-4061.

Bogrekci, I. and Godwin, R.J., 2007. Development of an image–processing technique for soil tilth sensing. Biosytems Engineering. 97, 323-331.

Bretar, F., Arab-Sedze, M., Champion, J., Pierrot-Deseilligny, M., Heggy, E., Jacquemoud, S., 2013. An advanced photogrammetric method to measure surface roughness: application to volcanic terrains in the Piton de la Fournaise, Reunion Island. Remote Sensing of Environment 135, 1-11.

Chimi-Chiadjeu, O., Vannier, E., Dusséaux, R., Le Hégarat-Mascle, S., Taconet, O., 2013. Using simulated annealing algorithm to move clod boundaries on seedbed digital elevation model. Comput. Geosci. 57, 68-76.

Chimi-Chiadjeu, O., Le Hégarat-Mascle, S., Vannier, E., Taconet, O., Dusséaux, R., 2014. Automatic clod detection and boundary estimation from digital elevation model images using different approaches. Catena 118, 73-83.

Choksi, P., 2018. Elementary theory of wavelets and filter bank. International Journal of Trend in Scientific Research and Development 2, 571-576.

Darboux, F., Davy, P., Gascuel-Odoux, C., Huang, C., 2001. Evolution of soil surface roughness and flowpath connectivity in overland flow experiments. Catena 46, 125-139.

Darboux, F., Huang, C. 2003. An instantaneous-profile laser scanner to measure soil surface microtopography. Soil Science Society of America Journal 67, 92-99.

Daubechies, I., 1992. Ten lectures on wavelets, in: CBMS Conf. Series in Appl. Math., Vol. 61, SIAM, Philadelphia.

De Oro, L.A., Buschiazzo, D.E., 2011. Degradation of the soil surface roughness by rainfall in two loess soils. Geoderma 164, 46-53.

Dusséaux, R., Vannier, E., Taconet, O., Granet, G., 2012. Study of backscatter signature for seedbed surface evolution under rainfall – Influence of radar precision. Progress In Electromagnetics Research 125, 415-437.

Fernandez-Diaz, J.C., Judge, J., Slatton, K.C., Shrestha, R., Carter, W.E., Bloomquist, D., 2010. Characterization of full surface roughness in agricultural soils using groundbased LIDAR. IGARSS July 25-30, 2010, Honolulu, Hawaï, USA.

Foster, G.R., Eppert, F.P. & Meyer, L. D. 1979. A programmable rainfall simulator for field plots. In: Proceedings of the Rainfall Simulator Workshop. Tucson, Arizona. March 7–9, 1979, pages 45–59, Sidney, Montana. Agricultural Reviews and Manuals, ARM-W-10. United States Department of Agriculture - Science and Education Administration, Oakland, CA.

Garbout, A., Munkholm, L.J., Hansen, S.B., 2013. Temporal dynamics for soil aggregates determined using X-ray CT scanning. Geoderma 204-205, 15-22.

Gilliot, J.M., Vaudour, E., Michelin, J., 2017. Soil surface roughness measurement: a new fully automatic photogrammetric approach applied to agricultural bare fields. Computers and Electronics in Agriculture 134, 63-78.

480 Haubrock, S. N.; Kuhnert, M.; Chabrillat, S.; Güntner, A.; and Kaufmann, H., 2009.
481 Spatiotemporal variations of soil surface roughness from in-situ laser scanning: *Catena*, vol.
482 79, pp. 128-139.

483 Jensen, T., Green, O., Munkholm, L.J., Karstoft, H., 2016. Fourier and granulometry methods
484 on 3D images of soil surfaces for evaluating soil aggregate size distribution. Applied
485 Engineering in Agriculture 32, 609-615.

486 Jester, W., Klik, A., 2005. Soil surface roughness measurement—methods, applicability and
487 surface representation. Catena 64, 174-192.

488 Josso, B., Burton, D.R., Lalor, M.J., 2001. Wavelet strategy for surface roughness analysis
489 and characterisation. Computer methods in applied mechanics and engineering 191, 829-
490 842.

491 Josso, B., Burton, D.R., Lalor, M.J., 2002. Frequency normalised wavelet transform for
492 surface roughness analysis and characterisation. Wear 252, 491-500.

493 Kamphorst, E.C., Jetten, V., Guérif, J., Pitkänen, J., Iversen, B.V., Douglas, J.T., Paz, A.,
494 2000. Predicting depressional storage from soil surface roughness. Soil Science Society
495 American Journal 64, 1749-1758.

496 Kamphorst, E.C., Chadoeuf, J., Jetten, V., Guérif, J., 2005. Generating 3D soil surfaces from
497 2D height measurements to determine depression storage. Catena, 62, 189-205.

498 Labarre, S., Ferrari, C., Jacquemoud S., 2017. Surface roughness retrieval by inversion of
499 the Hapke model: A multiscale approach. Icarus 290, 63-80.

500 Mallat, S. G., 1989. A theory for multiresolution signal decomposition: the wavelet
501 representation, IEEE transactions on pattern analysis and machine intelligence 11, 674-693.

502 Martinez-Agirre, A., Alvarez-Mozos, J., Gimenez, R., 2016. Evaluation of surface roughness
503 parameters in agricultural soils with different tillage conditions using a laser profile meter. Soil
504 and Tillage Research 161, 19-30.

505 Sandri, R., Anken, T., Hilfiker, T., Sartori, L., Bollhalder, H., 1998. Comparison of methods for
506 determining cloddiness in seedbed preparation. Soil and Tillage Research 45, 75-
507 90.Schapel, A., Marschner, P., Churchman, J., 2019. Influence of clay clod size and number
508 for organic carbon distribution in sandy soil with clay addition. Geoderma 335: 123-132.

509 Shen, F., and Zeng, G., 2019. Semantic segmentation via guidance of image classification.
510 Neurocomputing 330: 259-266.

511 Smith, M.W., 2014. Roughness in the Earth sciences. Earth Science Revue 136, 202-225.

512 Taconet, O., and Ciarletti, V., 2007. Estimating soil roughness indices on a ridge-and-furrow
513 surface using stereo photogrammetry. Soil and Tillage Research 93: 64-76.

514 Taconet, O., Vannier, E., Le Hégarat-Mascle, S., 2010. A boundary-based approach for
515 clods identification and characterization on a soil surface. Soil and Tillage Research 109,
516 123-132.

517 Taconet, O., Dusséaux, R., Vannier, E., Chimi-Chiadjeu, O., 2013. Statistical description of
518 seedbed cloddiness by structuring objects using digital elevation models. Computers &
519 Geosciences 60, 117-125.

520 Takken, I., Jetten, V., Govers, G., Nachtergaele, J., Steegen, A., 2001, The effect of tillage-
521 induced roughness on runoff and erosion patterns: *Geomorphology*, vol. 37, pp. 1-14.

522 Thomsen, L.M., Baartman, J.E., Barneveld, R.J., Starkloff, T., Stolte, J., 2015. Soil surface
523 roughness: comparing old and new measuring methods and application in a soil erosion
524 model. Soil 1, 399-410.

525 Vannier, E., Gademer, A., Ciarletti, V., 2006. A new approach for roughness analysis of soil
526 surfaces. EUSIPCO, September 4-8, 2006, Florence, Italy.

527 Vannier, E., Ciarletti, V., Darboux, F., 2009. Wavelet-based detection of clods on a soil
528 surface. Computers & Geosciences 35, 2259-2267.

529 Vannier, E., Taconet, O., Dusséaux, R., Chimi-Chiadjeu, O., 2014. Statistical
530 characterization of bare soil surface microrelief. In: Marghany, M. (Ed.), Advance geoscience
531 remote sensing. Edition Intech. Rijeka, Croatia, pp. 207-228.

532 Vannier, E., Taconet, O., Dusséaux, R., Darboux, F., 2018 a. A study of clod evolution in
533 simulated rain on the basis of digital elevation models. Catena 160, 212-221.

534 Vannier, E., Taconet, O., Dusséaux, R., Darboux, F., 2018 b. Using digital elevation models
535 and image processing to follow clod evolution under rainfall. Journal of Ecology and
536 Toxicology 2: 113.

537 Wang, W., Kravchenko, A.N., Smucker, A.J.M., Rivers, M.L., 2011. Comparison of image
538 segmentation methods in simulated 2D and 3D microtomographic images of soil aggregates.
539 Geoderma 162: 231-241.

540 Wang, B., Tang, S., Xiao, J.B., Yan, Q.F., Zhang, Y.D. 2019. Detection and tracking based
541 tubelet generation for video object detection. J. Vis. Commun. Image R. 58: 102-111.

542 Webb, A. R., 2002. Statistical pattern recognition, second edition. John Wiley & Sons, Ltd.
543 QinetiQ Ltd., Malvern, UK.

544 Zhang, L., Lu, Y., Lu, L., Zhou, T., 2019. Refined video segmentation through global
545 appearance regression. Neurocomputing 334: 59-67.

546 Zhao, L., Hou, R., Wu, F., Keesstra, S., 2018. Effects of soil surface roughness on infiltration
547 water, ponding and runoff on tilled soils under rainfall simulation experiments. Soil and
548 Tillage Research 179, 47-53.

549

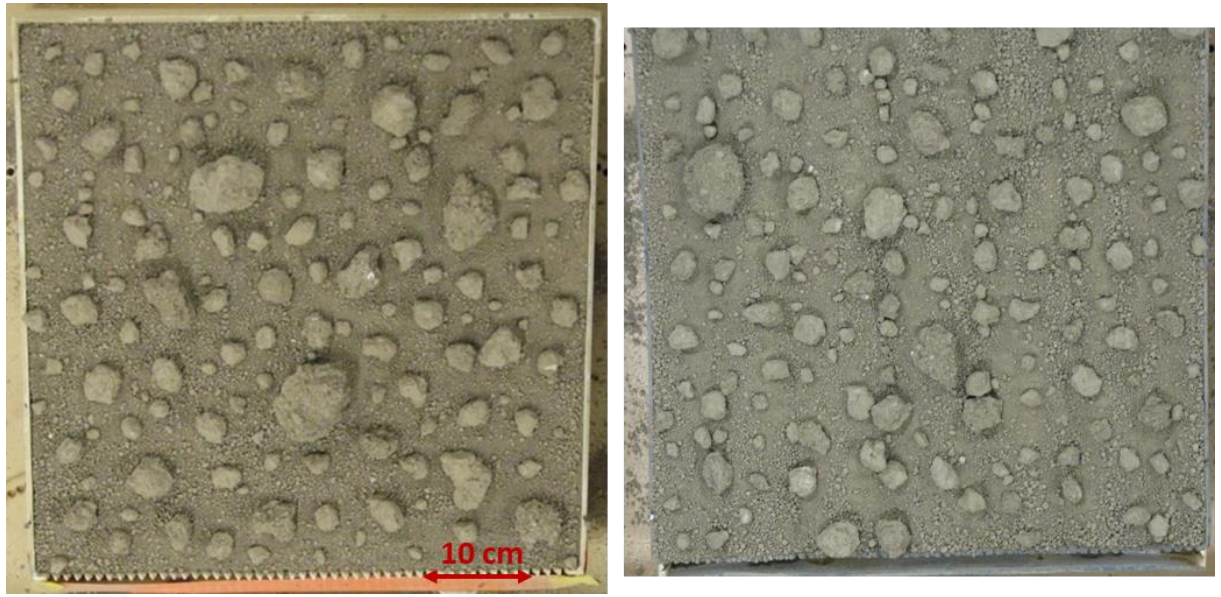

a) b)

Figure 1: Laboratory made planar and furrowed surfaces with a wide range of clod size P0 and F0.

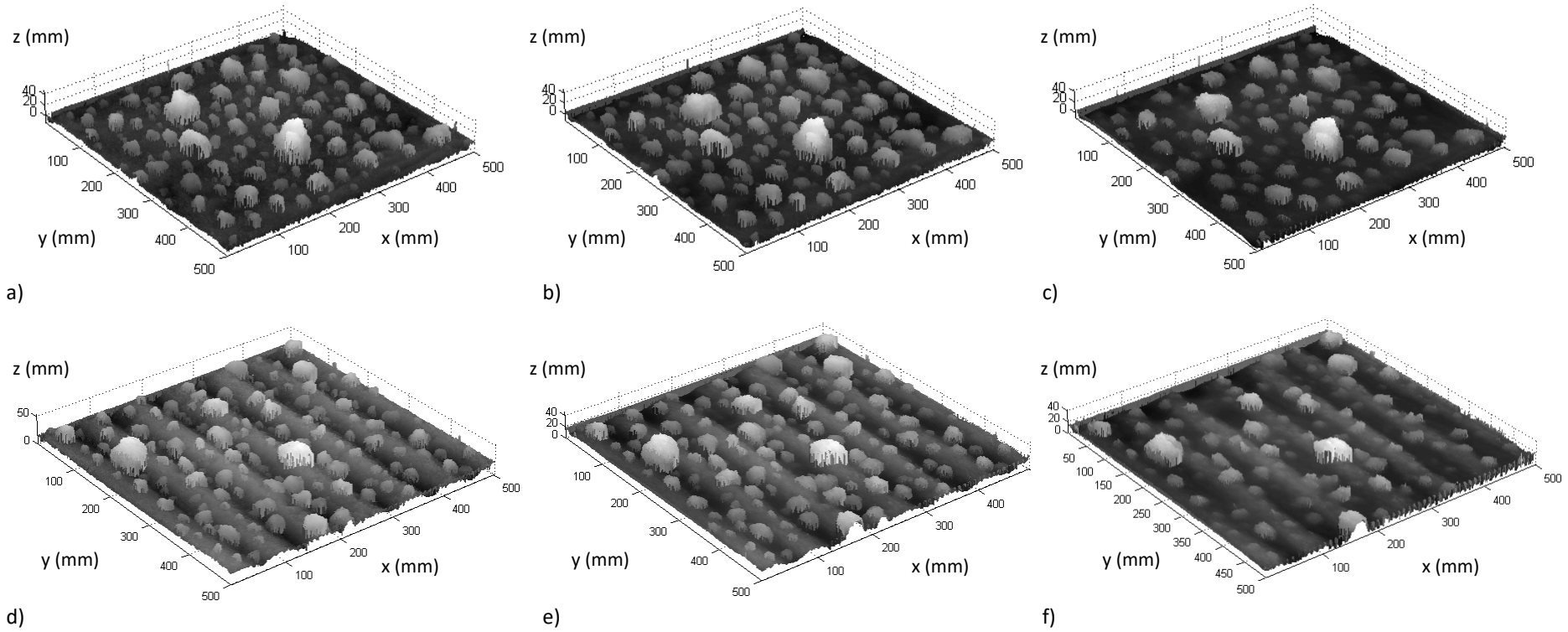

Figure 2: DEMs of planar and furrowed surfaces of wide range of clod size at initial and successive stages after rainfall; a) P0, b) P1, c) P2, d) F0, e) F1, f) F2.

a)

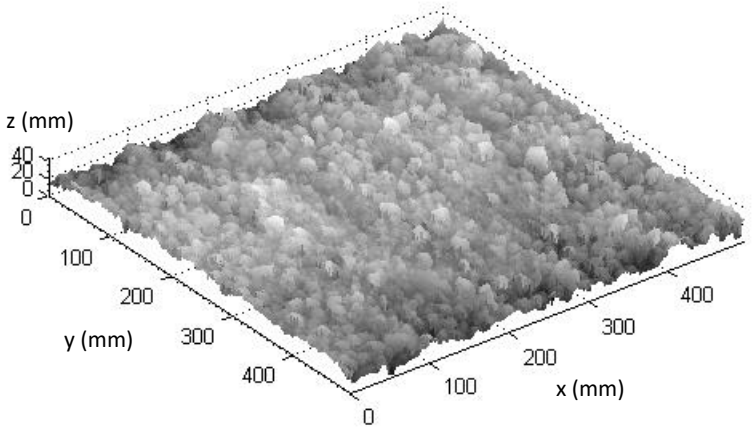

b)

Figure 3: Laboratory made and DEM of surface composed of one sieve range of clods SR.

For each detected clod,

1) Extract local surface around clod from DEM
$$SC = S(bx{:}ex,\ by{:}ey)$$
2) Remove mean plane of SC and get centered local surface SCf
3) Keep elevations above mean plane
$$MSC = SCf{>}0$$
4) Extract clod contour on clod mask MSC
5) Check goodness of intersection with mean plane and refine inclination and height of mean plane when needed
6) Check if local surface needs to be extended
7) Check for segmentation of a block of clods
8) Regularize clod contour by morpholigical opening (or closing for too small clods)
9) Rule out too flat clods
10) Correct or rule out squared clod contours.

Sort validated clod contours by decreasing size.

For each validated clod contour,

Check for inclusion or partial overlapping with other clod contours. Remove included clods and redelineate overlapping contours.

Figure 4: Algorithm of wavelet-based clod segmentation method. [*bx ex by ey*] represent the extents of the local surface in the directions *x* and *y*.

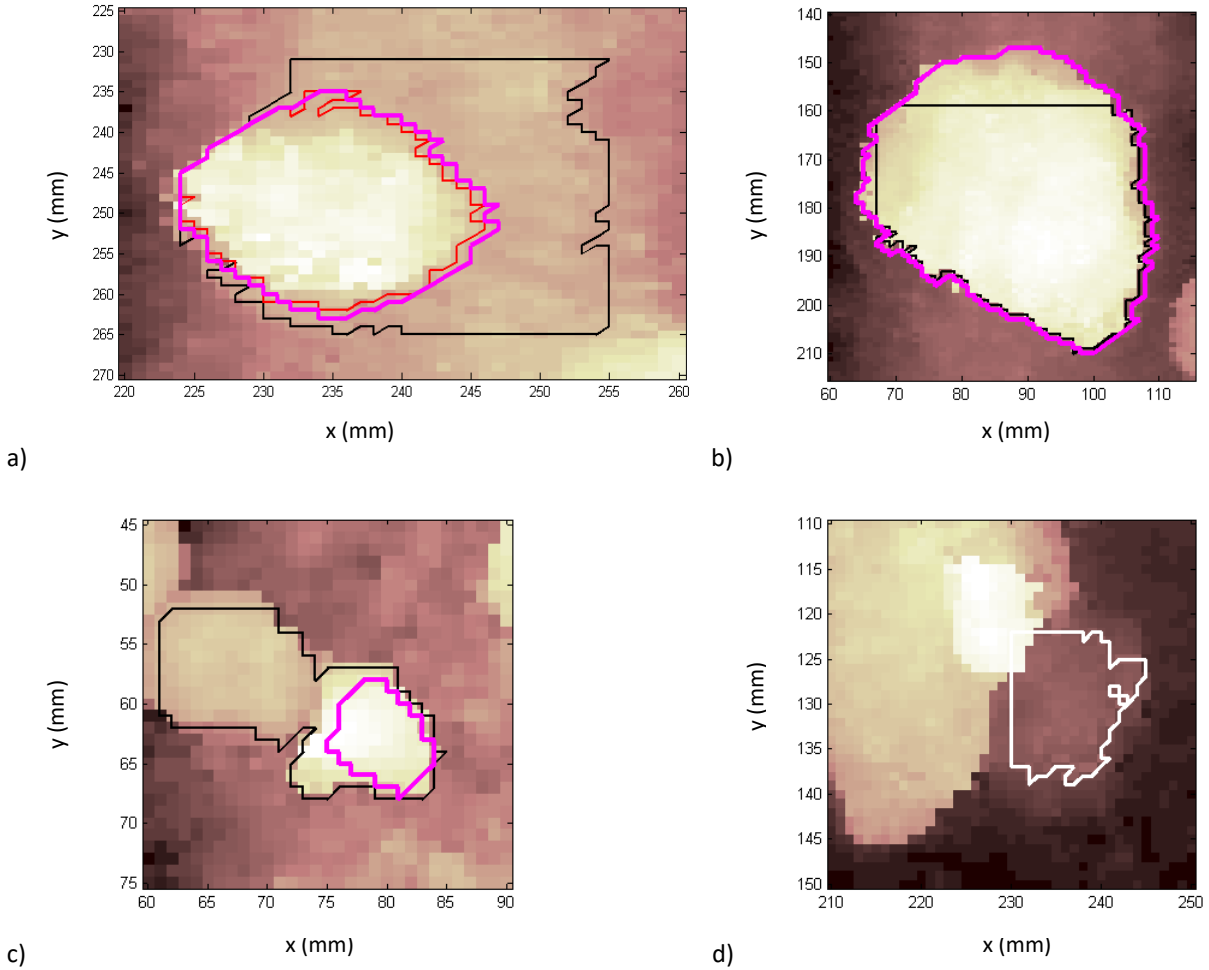

Figure 5: Rectification of wrong patterns encountered during clod contours automatic delineation. Initial contour is in black (a, b, c) or white (d), final contour in red (a) and regularized contour in bold magenta (a, b, c, d).

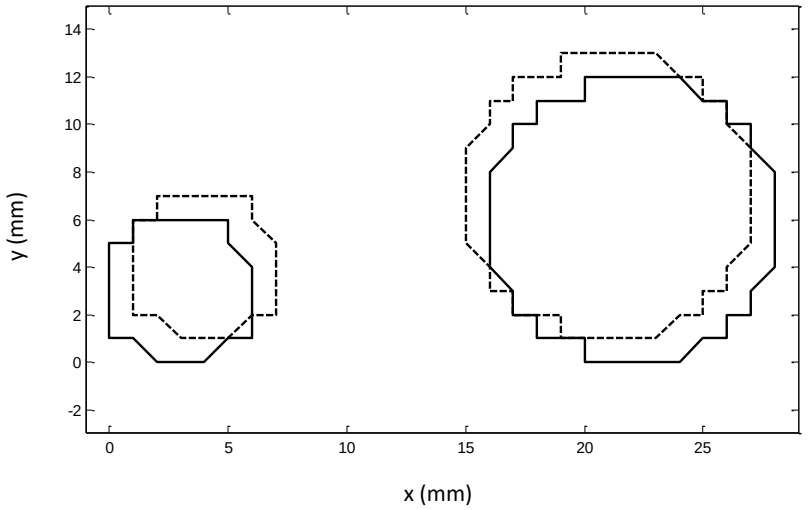

Figure 6: Dependence on clod size and DEM accuracy of goodness of agreement indicator. Discretized circles of 3 mm and 6 mm of radius (solid line) and translated circles by 1 mm (dotted line).

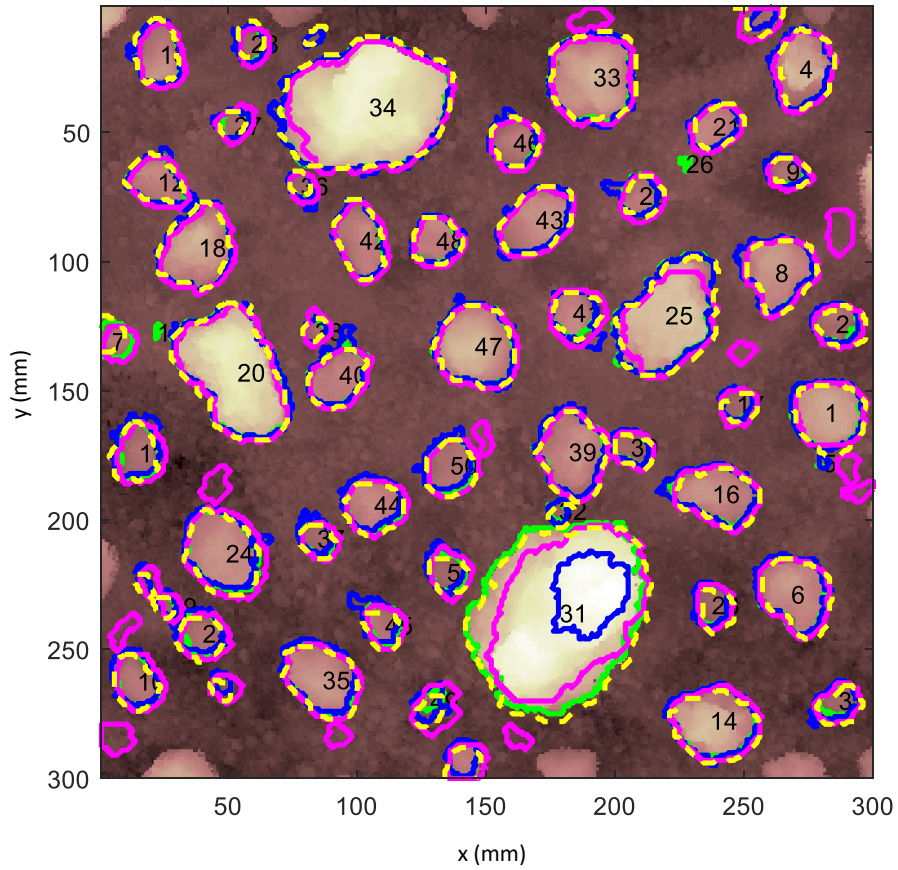

Figure 7: Clod contours obtained with hand-made segmentation (dotted yellow), thresholding (green), contour-based segmentation (blue) and wavelet-based segmentation (magenta) for planar surface at initial stage (P0).

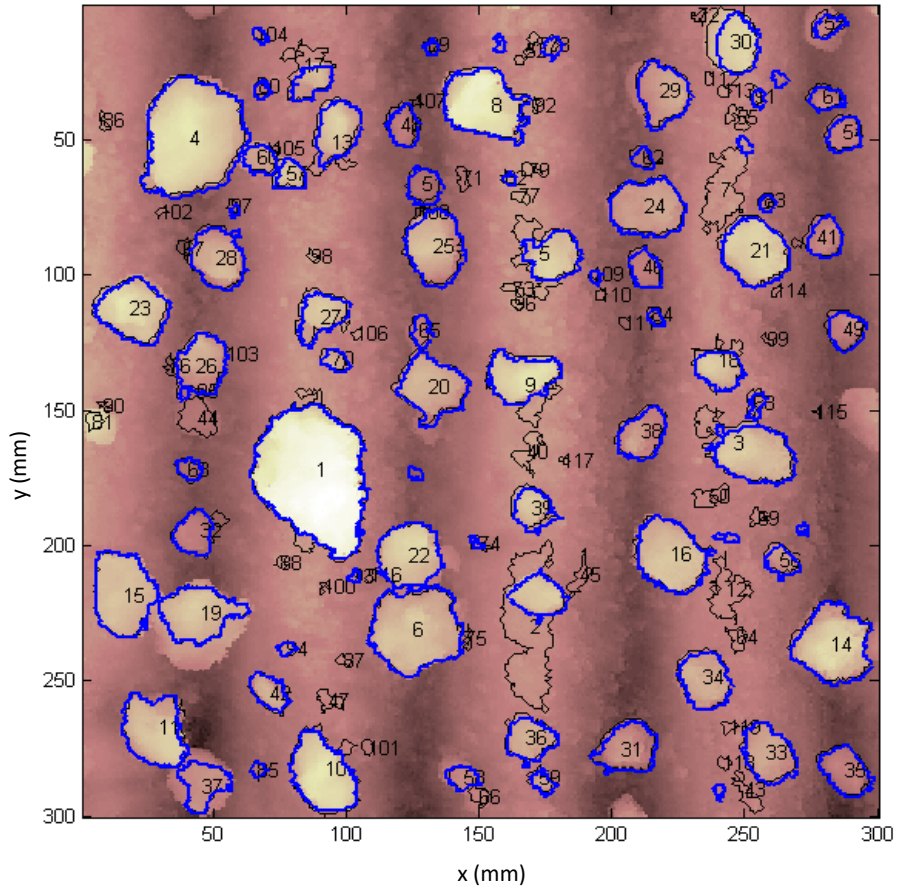

Figure 8: Clod contours obtained with contour-based segmentation without detrending (black) and after detrending (bold blue) for furrowed surface at initial stage (F0).

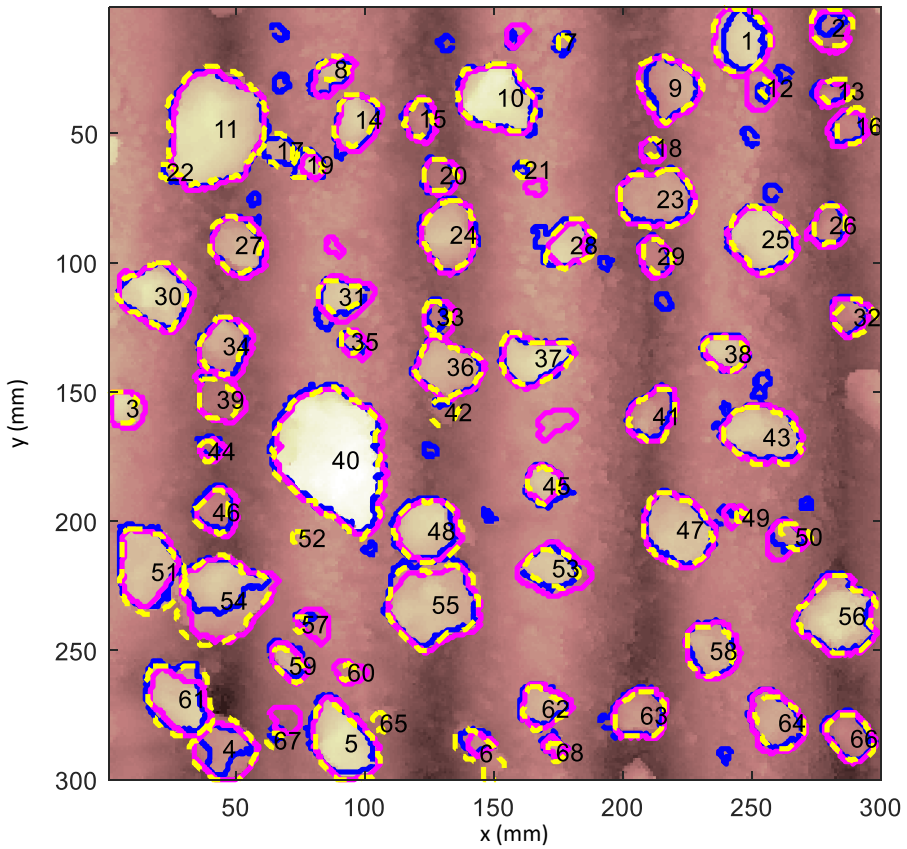

Figure 9: Clod contours obtained with hand-made segmentation (dotted yellow), contour-based segmentation after detrending (blue) and with wavelet-based segmentation (magenta) for furrowed surface at initial stage (F0).

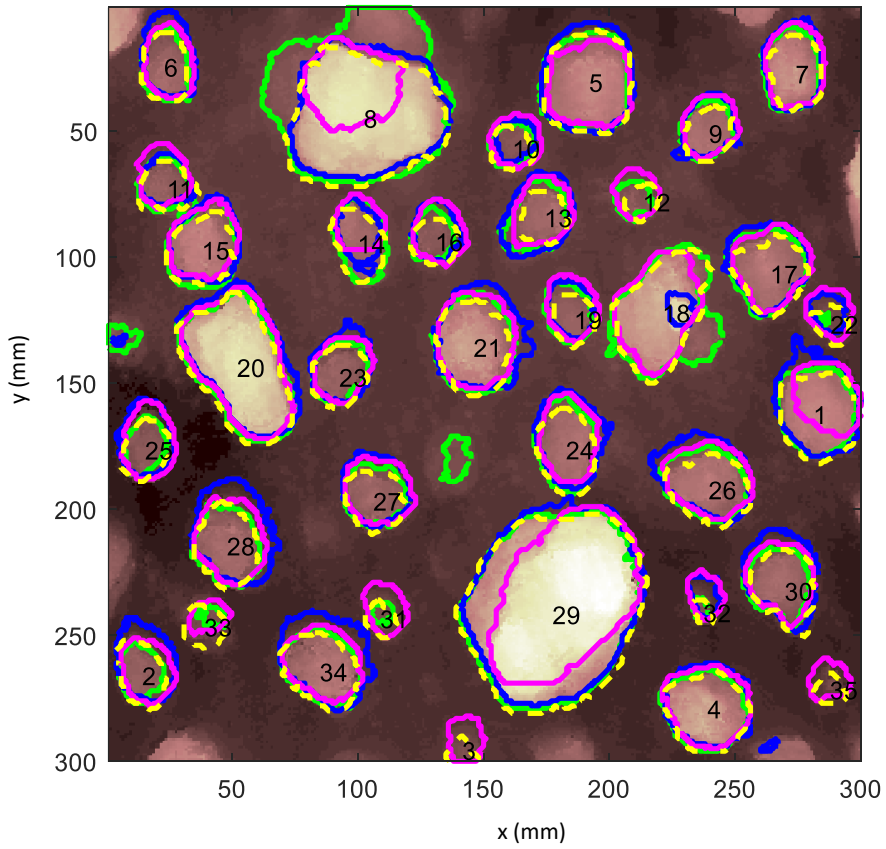

Figure 10: Clod contours obtained with hand-made segmentation (dotted yellow), thresholding (green), contour-based segmentation (blue) and wavelet-based segmentation (magenta) for planar surface after two rainfall events (P2).

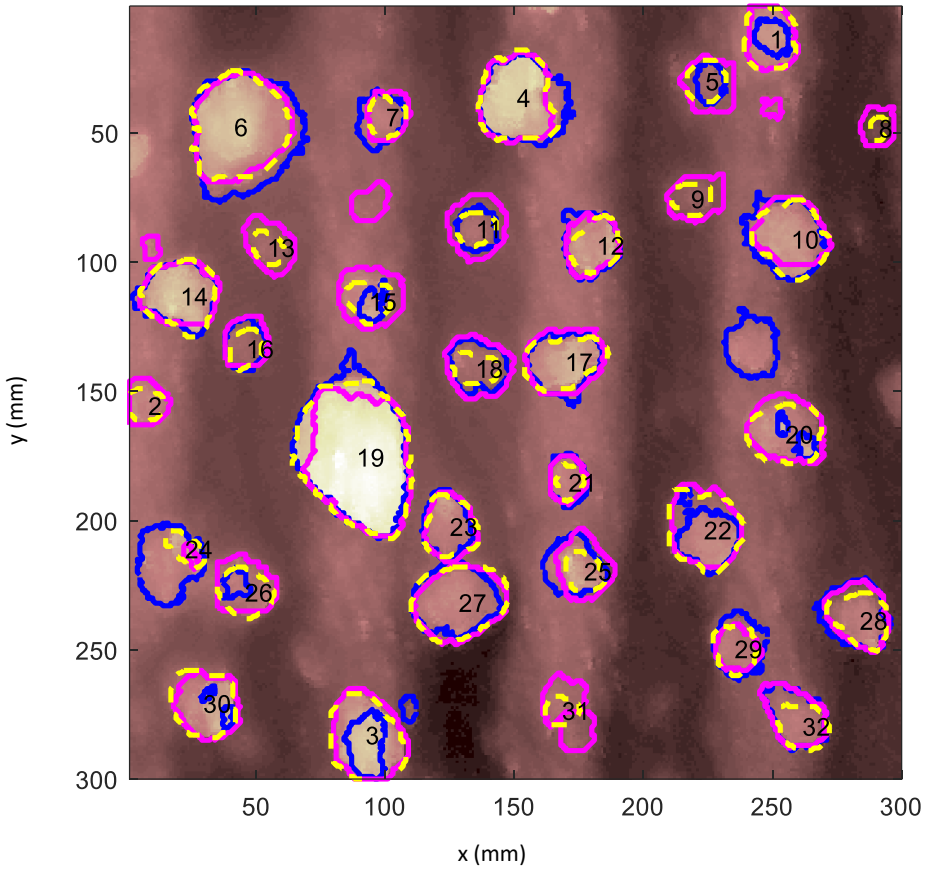

Figure 11: Clod contours obtained with hand-made segmentation (dotted yellow), contour-based segmentation after detrending (blue) and with wavelet-based segmentation (magenta) for furrowed surface after two rainfall events (F2).

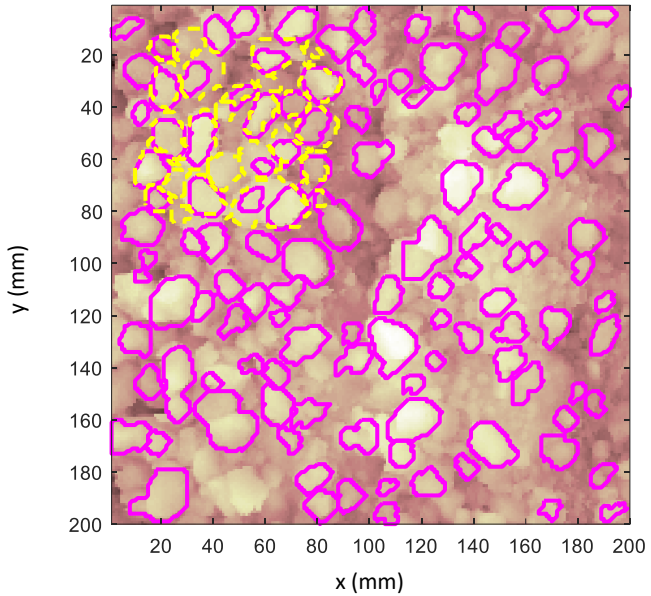

Figure 12: Results of wavelet-based segmentation (in magenta) on small size clod surface SR, with hand-made contours in dotted yellow.

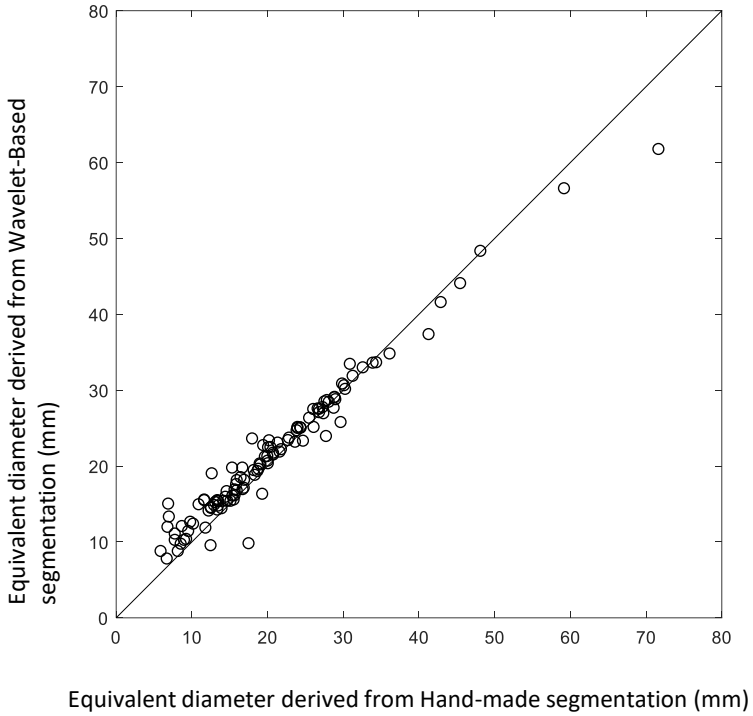

Figure 13: Clod diameters estimated from wavelet-based and hand-made segmentations on laboratory surfaces at initial stage P0 and F0.

			Compared method	
Reference	**Surface**	Threshold	Contour-Based	Wavelet-Based
Hand-made	P0	81.7	74.8	78.0
	P1	82.0	70.4	73.5
	P2	71.2	61.5	61.5
	F0		68.8*	70.2
	F1		74.6*	75.5
	F2		54.7*	66.1
Threshold	P0		85.5	74.5
	P1		73.4	74.6
	P2		64.4	65.8
Contour-Based*	P0			69.4
	P1			79.9
	P2			73.5
	F0			69.6
	F1			79.4
	F2			55.1

Table 1: Mean IoU in %, for three stages of planar surface P0 to P2 and furrowed surface F0 to F2. *from a detrended surface.

		Segmentation method		
Surface	Hand-made	Threshold	Contour-Based	Wavelet-Based
P0	29.5	27.9	26.4	30.5
P1	36.7	34.4	37.7	36.8
P2	28.4	30.7	30.9	26.7
F0	24.0		23.3*	25.6
F1	27.9		26.3*	28.2
F2	16.5		16.5*	19.7

Table 2: Clod coverage in %, for three stages of planar surface P0 to P2 and furrowed surface F0 to F2. *from a detrended surface.

	Segmentation method			
Surface	Hand-made	Threshold	Contour-Based	Wavelet-Based
P0	37.5	37.4	31.4	33.0
P1	39.9	41.4	41.6	36.9
P2	41.9	44.9	42.8	34.7
F0	26.6		25.9*	26.4
F1	30.8		30.1*	30.1
F2	30.5		31.8*	29.1

Table 3: Mean weighted diameter (MWD) in mm, for three stages of planar surface P0 to P2 and furrowed surface F0 to F2. *from a detrended surface.

		Compared method		
Reference	**Surface**	Threshold	Contour-Based	Wavelet-Based
Hand-made	P0	88.2	83.8	83.9
	P1	87.8	77.4	77.6
	P2	79.7	69.9	65.1
	F0		78.3*	81.6
	F1		81.1*	81.9
	F2		62.2*	78.2
Threshold	P0		91.7	80.7
	P1		78.9	78.3
	P2		72.0	66.7
Contour-Based*	P0			77.2
	P1			81.9
	P2			72.5
	F0			80.0
	F1			86.1
	F2			70.8

Table 4: Goodness of agreement (in %) between segmentation methods, for three stages of planar surface P0 to P2 and furrowed surface F0 to F2. *from a detrended surface.